NEXRES 12 (2026) 102266

Contents lists available at ScienceDirect

Next Research

journal homepage: www.elsevier.com/locate/nexres

Research Paper

One-sided predictive thresholds for aerospace electromechanical actuators: Monte Carlo and probability-plot methods

Fawaz Yahya Annaz *

Birmingham City University, The School of Engineering and the Built Environment Millennium Point, Curzon Street, Birmingham B4 7XG, United Kingdom

ARTICLE INFO

Keywords:
Electromechanical actuators
Fault detection and isolation
Threshold setting
Monte Carlo
Probability plots
Lognormal modelling
Aerospace
Voter logic

ABSTRACT

Electromechanical actuators (EMAs) on flight-critical surfaces require defensible, auditable thresholds for lane-level monitoring and fault isolation. The approach is broadly applicable and is demonstrated on an output-summed, multi-lane Sea Harrier EMA with continuous lane monitoring and voting. Monte Carlo sampling of motor and sensor tolerances drives simulations to estimate peak lane disparity distributions for current, potentiometer, and tachometer signals across Mach 0–1 and the commanded-deflection envelope under inertial and aerodynamic loading. Normal and lognormal probability plots provide visual diagnostics and guide tail-model selection between two and three parameter lognormal forms. The workflow aligns the classical straight-line probability-paper practice with automated lognormal fitting to set one-sided predictive thresholds at a 10^{-4} nuisance-disconnect (healthy false-alarm) target per operating point, while quantifying model-choice effects (Linear, 2-parameter lognormal, 3-parameter lognormal) and their impact on conservatism at very low probabilities. The procedure produces traceable, tool-based thresholds that suit industrial needs for repeatability and auditability in voter-logic architectures. Results show that three-parameter lognormal modelling can add useful conservatism in the extreme tail. Automated lognormal fitting also provides a practical foundation for AI-based, predictive threshold setting that adapts to evolving operating conditions. Overall, the workflow yields certifiable thresholds for aerospace applications, where transparency of assumptions and protection against rare events are as critical as detection performance.

List of acronyms and symbols

Acronyms	
EMA	Electromechanical Actuator
PLD	Peak Lane Disparity
FDI	Fault Detection and Isolation
PDF	Probability Density Function
CDF	Cumulative Distribution Function (appears in lognormal modelling)
AI	Artificial Intelligence
CI	Confidence Interval (95% binomial CIs)
Flight cases / actuator operating point	
$\delta_a{}^o$	Aileron Deflection
M	Mach number $0.2 \le M \le 1.0$
Simulation setup / sampling	
n	Sample size (for example 1500)
α	Nuisance-disconnect design target per operating point (10^{-4})
$\widehat{p}$	Observed false-alarm rate.
Peak lane disparity (PLD) notation	
PLD_{max}	Maximum observed peak lane disparity in the dataset.
$IPLD(\delta, M)_i$	PLD from the ith simulation at flight case.
Binning / empirical distribution construction	
Δx	Interval width
EC_j	Event count in the j^{th} interval
$EC_{count,1\sim n}$	Event count for 100 bins.
$\%P_i$	Cumulative percentage up to the i^{th} interval
Monte Carlo integration	
N_H	Number of "hits" (points under curve)
Lognormal modelling / probability plots	
μ, σ	Lognormal parameters (mean, std in log-space).
$\Phi(\cdot)$	Standard normal CDF (appears in lognormal CDF)

Introduction

Electromechanical actuators (EMAs) used on flight-critical control surfaces require defensible threshold values for lane-level monitoring and fault isolation. In redundant or multi-lane architectures, these

* Corresponding author at: Birmingham City University, The School of Engineering and the Built Environment, Millennium Point, Curzon Street, Birmingham B4 7XG, United Kingdom.

E-mail address: fawaz.annaz@bcu.ac.uk.

https://doi.org/10.1016/j.nexres.2026.102266
Received 18 July 2026; Accepted 1 August 2026
Available online 3 August 2026

thresholds must distinguish healthy internal disparities from abnormal behaviour without causing excessive nuisance disconnects. If thresholds are set too low, healthy lanes may be unnecessarily isolated, reducing availability and potentially compromising fault-tolerant operation. If thresholds are set too high, significant internal disparities may remain undetected, allowing degraded behaviour to persist and increasing the risk of unsafe operation. Threshold setting is therefore a central problem in the design and certification of voter-based monitoring systems for aerospace EMAs [1,2].

In practice, threshold selection is complicated by the fact that actuator behaviour depends strongly on operating conditions, including flight speed, commanded surface deflection, loading, and uncertainty in motor and sensor tolerances. Fault detection and isolation (FDI) methods for EMAs have been widely investigated, and monitoring schemes based on currents, position sensors, and speed sensors are common in multi-lane architectures [3–5] . However, the practical problem of how to set threshold values in a transparent, repeatable, and auditable manner remains challenging, particularly when thresholds must be scheduled across the operating envelope. In many engineering settings, empirical data are plotted on probability paper, a straight line or curve is fitted manually, and the result is extrapolated to obtain a threshold at a chosen occurrence probability. While intuitive, this classical procedure is subjective, difficult to reproduce, and poorly suited to systematic threshold scheduling.

Monte Carlo simulation provides a natural means of generating empirical data under uncertainty and is well suited to modelling the combined effects of component tolerances, loading, and operating-point variation. In the present context, it is used to generate peak lane disparity (PLD) data for monitored signals such as motor current, potentiometer output, and tachometer response across the flight envelope. The contribution of this paper is not the use of Monte Carlo in itself, since Monte Carlo methods are already established in fault detection and uncertainty analysis [3,5]. Rather, the focus is on how Monte Carlo-generated PLD data can be translated into threshold values through a structured, probability-plot-based workflow that preserves the engineering intuition of traditional probability-paper methods while removing their manual and subjective elements.

Accordingly, this paper presents a one-sided predictive threshold-setting methodology for aerospace EMAs in which Monte Carlo-derived PLD data are analysed using normal and lognormal probability plots to derive operating-point-dependent threshold values. The method is demonstrated on an output-summed, multi-lane Sea Harrier EMA with continuous lane monitoring and voting [2,4]. The paper makes three principal contributions. First, it formalises the traditional manual probability-paper threshold-setting logic into a reproducible, tool-based workflow. Second, it compares linear, two-parameter lognormal, and three-parameter lognormal tail models in order to show how model choice affects conservatism at very low probabilities. Third, it demonstrates how the resulting thresholds can be scheduled across the operating envelope in a voter-based aerospace EMA context. In this way, the paper aims to show not only how thresholds may be estimated, but how they may be set in a form that is more systematic, auditable, and practically useful for engineering applications.

Monte Carlo-basedthreshold-settingframework

The purpose of the Monte Carlo analysis in this paper is not to review Monte Carlo methods in general, but to generate empirical peak lane disparity (PLD) data under uncertainty for threshold setting in a multi-lane aerospace electromechanical actuator. The workflow uses repeated simulations in which motor and sensor tolerances are sampled across the actuator operating envelope. For each operating point, the resulting distributions of PLD in monitored signals, namely current, potentiometer, and tachometer outputs, are used to derive one-sided predictive thresholds at a specified nuisance-disconnect probability [6–8].

In this context, Monte Carlo simulation serves as a practical means of propagating uncertainty in actuator and sensor parameters into observable monitoring quantities. Each simulation run represents one admissible realisation of the system under a given flight condition. Repeating this process across a sufficiently large number of runs produces the empirical PLD distributions that form the basis for threshold extraction using probability-plot methods. The role of Monte Carlo is therefore strictly operational: it provides the data required for threshold estimation rather than constituting the principal contribution of the paper.

The threshold-setting logic follows the classical engineering idea of plotting empirical data on probability paper and extrapolating the fitted trend to a target occurrence level. However, instead of relying purely on manual plotting and subjective curve fitting, the present workflow combines simulation-generated empirical distributions with explicit model selection between linear, two-parameter lognormal, and three-parameter lognormal tail representations. In this way, the procedure preserves the interpretability of traditional probability-paper methods while improving repeatability, auditability, and suitability for operating-point-dependent threshold scheduling [9].

Only the elements of Monte Carlo analysis directly required for this workflow are therefore retained in the revised manuscript: random sampling of tolerances, generation of PLD datasets across operating conditions, construction of empirical cumulative distributions, and extraction of one-sided predictive thresholds from the fitted tails. General Monte Carlo derivations and broader algorithmic variants that are not explicitly used in the proposed methodology have been removed in order to maintain focus on the EMA threshold-setting problem.

Methodology: graphicalmonteCarlothresholdestimationon normaland lognormalmodels

Building upon the probabilistic modelling and graphical threshold estimation techniques discussed earlier, this section presents a practical application of the method, referred to as the simulation graphical Monte Carlo, for setting sensor thresholds in fault-tolerant electromechanical actuator systems. Following the characterisation of empirical distributions and the use of probability paper [9] to visualise and extrapolate threshold levels, this method operationalises those concepts by incorporating simulation data, statistical binning, and graphical interpretation [6]. The aim is to derive threshold values that balance sensitivity and false alarm tolerance within real-world actuator monitoring architectures.

Aerospace EMA systemand monitoringcontext

The case study considered in this paper is an output-summed, multi-lane electromechanical actuator (EMA) representative of an aerospace flight-control application. The actuator is associated with the Sea Harrier inboard aileron and operates across a flight envelope defined by commanded aileron deflection, Mach number, inertial loading, and aerodynamic loading. The purpose of the case study is not to report hardware testing, but to provide a realistic aerospace context in which threshold-setting requirements can be examined systematically.

The monitoring quantities considered are motor current, potentiometer output, and tachometer response. These signals are used within a fault detection and isolation (FDI) framework in which lane disparities are monitored continuously and abnormal deviations can trigger fault indication and lane isolation. In healthy operation, some degree of mismatch between lanes is expected because of tolerances, loading variation, and operating-point dependence. The threshold-setting problem is therefore to distinguish acceptable healthy disparities from disparities large enough to justify a fault indication or nuisance disconnect.

Fig. 1 identifies the Sea Harrier aileron application considered in this study, while Fig. 2 illustrates the monitoring-voting-averaging logic that

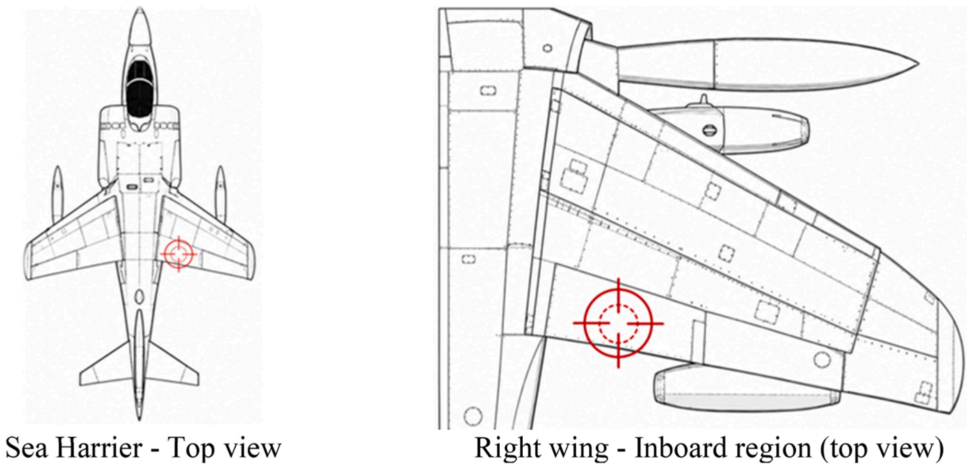

Fig. 1. Top view of the Sea Harrier showing the inboard aileron considered in this study.

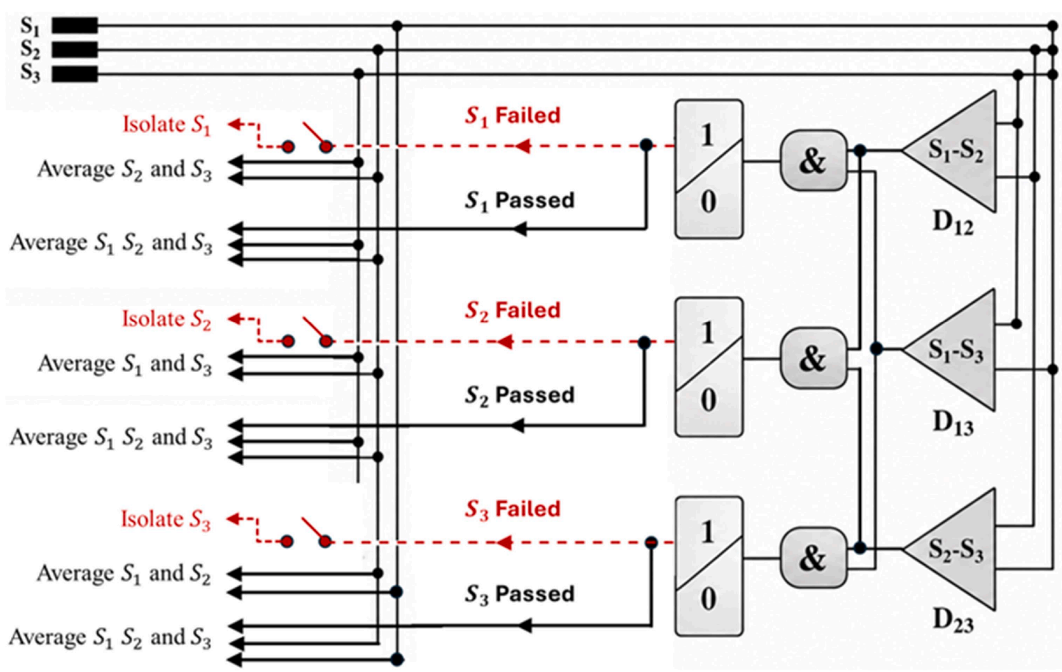

Fig. 2. Schematic of the monitoring-voting-averaging logic used in the multi-lane EMA.
The system compares lane signals, evaluates pairwise disparities, isolates abnormal components or lanes, and returns the average of the remaining active signals. Threshold setting in this paper is based on healthy peak lane disparity distributions of motor current, potentiometer output, and tachometer response.

links lane-disparity thresholds to practical fault detection and isolation decisions. The actuator and aircraft constraints assumed in the case study include the Sea Harrier-like operating envelope, aileron authority limits, manoeuvre requirements, and acceptable aircraft response to failure transients. Table 1 summarises the main aircraft and actuator specifications that define the operating envelope and response limits used in the present threshold-setting study.

These specifications define the operating region and response limits within which the threshold-setting methodology is applied. In particular, the nuisance-disconnect target and the acceptable aircraft response to failure transients provide the engineering context for selecting one-sided predictive thresholds from the healthy PLD distributions.

In the present study, actuator behaviour is examined through simulation rather than hardware experimentation. The purpose of the case study is therefore methodological: to demonstrate how threshold values can be derived in a systematic and reproducible way from simulated lane-disparity data across the operating envelope. This allows the threshold-setting process itself to be examined clearly while retaining direct relevance to aerospace EMA monitoring practice.

The actuator and aircraft constraints assumed in the case study include the Sea Harrier-like operating envelope, aileron authority limits, manoeuvre requirements, and acceptable aircraft response to failure transients. Table 1 summarises the main aircraft and actuator specifications used in the present threshold-setting study.

Threshold-setting problemformulation

For each monitored signal, the quantity of interest is the peak lane disparity (PLD) obtained from repeated simulations at a given operating point. PLD represents the maximum observed internal difference between actuator lanes for that signal under the simulated flight condition. In practical terms, it provides a compact measure of the worst healthy internal lane mismatch that a voter or monitoring function may have to tolerate in healthy operation. Threshold values are then set on the basis

Table 1
Main aircraft and actuator specifications defining the operating envelope and acceptable response limits used in the present threshold-setting study.

Aircraft	
Parameter	Value / Requirement
Speed range	Mach $0.2 \le M \le 1.0$
Maximum aileron authority (with linear variation at intermediate speeds)	at $M = 0.2; \delta_a = \pm 18^{\circ}$ at $M = 1.0 \rightarrow \delta_a = \pm 2^{\circ}$
Maximum manoeuvre	0 to $+5.0g$
Maximum allowable bank angle due to first failure transient	3^{o}
Maximum allowable roll rate due to first failure transient	$5^{o}s^{-1}$

Actuator	
Parameter	Value / Requirement
Architecture	Multi-lane torque-summed output
Maximum rotary output	$\pm 18.0^{o}$
Minimum output rate	0.5 rad s $-$ 1
Bandwidth	8 Hz at 1°, based on $-$ 3dB at 5% of maximum output amplitude
Load capability	Capable of driving inertial and aerodynamic loads
Nuisance-disconnect requirement	Probability of first nuisance disconnect $< 1.0 \times 10^{-4}$
Fault-tolerance requirement	Capable of driving inertial and aerodynamic loads adequately after two lane failures

of these PLD distributions.

The engineering objective is to select thresholds that balance two competing requirements. If thresholds are too low, the actuator monitoring system will generate excessive nuisance disconnects or false fault indications. If thresholds are too high, significant internal disparities may remain undetected, reducing the sensitivity of the monitoring scheme. In this study, the design target is a one-sided nuisance-disconnect probability of 10^{-4} per operating point, so the threshold is taken from the upper tail of the healthy PLD distribution.

Traditionally, such thresholds may be estimated by plotting empirical data on probability paper, fitting the trend manually, and extrapolating to the desired occurrence level. The limitation of that approach is that it depends strongly on analyst judgement and is difficult to reproduce consistently across many operating points. The present paper addresses this limitation by using Monte Carlo-generated PLD data together with normal and lognormal probability-plot models to define thresholds in a more structured and auditable way.

Simulation procedure

The primary aim of the simulation graphical Monte Carlo procedure [6] is to establish statistically valid threshold values for motor-current, potentiometer, and tachometer signals within a global FDI system. These monitored signals also support voter logic, enabling the identification and isolation of failed components while returning the average feedback from the remaining active units. Fig. 3 summarises the workflow used to derive one-sided predictive thresholds at a nuisance-disconnect probability of $\alpha = 10^{-4}$ per operating point.

If thresholds are set too low, the monitoring system becomes prone to false alarms and nuisance disconnects; if they are set too high, significant internal disparities may remain undetected. The simulation graphical Monte Carlo procedure is therefore used to generate empirical PLD distributions across the operating envelope, from which thresholds can be selected to balance detection sensitivity against false-alarm risk.

The simulation procedure used to generate the empirical PLD distributions for threshold setting is summarised as follows.

1. Identify a sample size (n) that gives confidence in the obtained results, say $n = 1500$.
2. For a given flight case, defined by aileron deflection δ_a and Mach number M, determine the PLD from each simulation run. Let $I_{PLD(\delta_a,M)_i}$ denote the PLD obtained from the i^{th} simulation at that

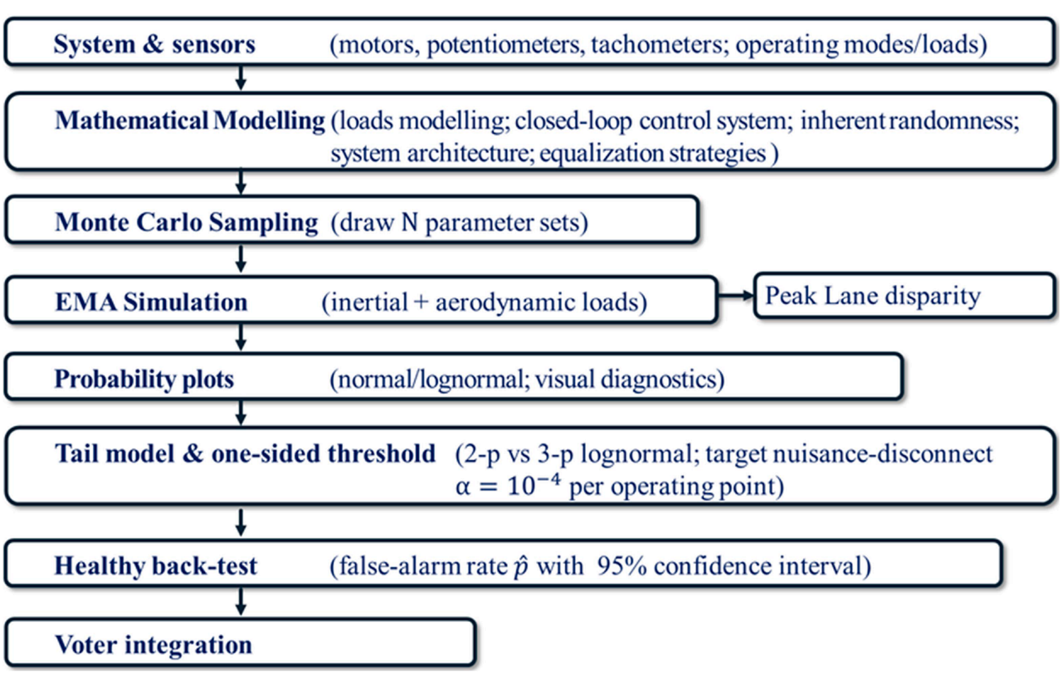

Fig. 3. An overview of the threshold-setting workflow.
System and modelling inputs feed Monte Carlo sampling and EMA simulation. Each run yields the peak lane disparity (current, potentiometer, tachometer). Probability plots diagnose fit and guide 2 vs 3 parameter lognormal tail modelling. A one-sided threshold is set at the target nuisance-disconnect probability $\alpha = 10^{-4}$ per operating point and validated on independent healthy simulations (observed false-alarm rate $\hat{p}$ with 95% confidence interval), then integrated with lane-voter logic.

operating point, where the disparity arises from the internal lane random variations.

3. Repeat this process across the flight envelope accounting for variations in aileron deflection and Mach number ($18^o \geq \delta \geq 2^o$ and $0.2 \leq M \leq 1$), and record the PLD values for each operating point.
4. Construct a data bank comprising all peak lane disparities, arranged from zero to the maximum observed value PLD_{max}.
5. Divide the data into intervals Δ_x (with each interval having equal or adaptive width and arrange from zero to PLD_{max}, as shown in the 1st column of Table 1.
6. Count the number of events that fall within each interval. Table 1 assumes 100 intervals ($\Delta_1 \Delta_{100}$), as shown in the second column. The third column lists the corresponding event counts. Let EC_jdenote the event count in the j^{th}interval. For the typical data in Table 2, this may be written as: $1 : [0, 0.5)$; $88 : [0.5, 1.0)$; $244 : [1.0, 1.5)$; etc Table 1a.

1. Compute the cumulative sum of event counts across the intervals to form the cumulative distribution.
2. Calculate the cumulative percentage probability for each interval using

$$\%P_i = 100 \frac{\sum_{k=1}^{j} EC_k}{N} \tag{1}$$

3. Plot the percentage probabilities on probability graph paper against the upper bound of each interval on normal probability paper, as shown in Fig. 4. The x-axis represents the percentage probability, while the y-axis represents the upper interval limit, which corresponds to the threshold-value axis [9].
4. If scheduled thresholds are required, repeat Steps 1–9 across the flight envelope to calculate thresholds at the target probability level of $10^{-4}$for each operating point. These thresholds are then scheduled according to the relevant flight case, as shown in the flowchart in Fig. 5.
5. If a single unscheduled threshold is required, select the maximum threshold calculated across the flight envelope and apply it to all flight cases, as shown in Fig. 5.

Threshold estimationon normalprobabilitypaper

The primary aim of applying the simulation graphical Monte Carlo method is to determine statistically sound threshold values for devices monitoring motor currents, potentiometer outputs, and tachometer readings within a global fault detection and isolation (FDI) system [10]. These monitoring devices also function as voters, identifying and isolating failed components while returning the average value from the remaining operational units. This arrangement is consistent with actuator characterisation and voting practices reported in NASA flight-programme testing [11].

Table 1a
Setting up the Simulation Graphical Monte Carlo.

Data bank	Interval (Δ)	Events count (EC)	Cumulative Sum (CS)	Probability percentage of occurrence (%P)
$\boldsymbol{I}_{\boldsymbol{PLD}(18^o,0.2)_0}$	0	EC_1	$E_{count\,1}$	$P_1 = \frac{E_{count\,1}}{1500} \times 100$
$\boldsymbol{I}_{\boldsymbol{PLD}(18^o,0.2)_1}$	Δ_1	EC_2	$\sum_0^1 E_{count\,i}$	$P_2 = \frac{\sum_0^1 E_{count\,i}}{1500} \times 100$
$\boldsymbol{I}_{\boldsymbol{PLD}(18^o,0.2)_k}$	Δ_k	EC_k	$\sum_1^k E_{count\,i}$	$P_{99} = \frac{\sum_1^k E_{count\,i}}{1500} \times 100$
$\boldsymbol{I}_{\boldsymbol{PLD}(18^o,0.2)_{99}}$	Δ_{99}	EC_{99}	$\sum_1^{99} E_{count\,i}$	$P_{99} = \frac{\sum_1^{99} E_{count\,i}}{1500} \times 100$

For each monitored signal, the empirical PLD data obtained from the simulation procedure are arranged into intervals and converted into cumulative occurrence probabilities. These empirical probabilities are then plotted against the corresponding upper interval limits on normal probability paper. This provides an interpretable graphical representation of the healthy PLD distribution and supports initial threshold estimation from the upper tail.

Thresholds set too low lead to excessive false alarms or nuisance disconnects, whereas thresholds set too high may fail to detect significant internal disparities. In aerospace applications, thresholds are often designed to allow nuisance disconnects with a probability as low as 10^{-4} [12]. If the plotted data lie approximately on a straight line, the underlying PLD distribution may be treated as approximately normal over the region of interest. In such cases, the threshold corresponding to a target false alarm probability, such as 0.1%, can be determined by extending the fitted line to the corresponding point on the probability axis.

Normal probability paper therefore provides the baseline graphical framework for threshold estimation before alternative tail models are considered. In the present workflow, it is not treated as the final answer in all cases, but as the first stage in the threshold-setting process, against which departures from linearity and possible improvements from lognormal tail modelling can be assessed.

The percentage probability scale is displayed along the top axis of the probability graph paper and complements the bottom x-axis. For instance, a value of 99.9% on the bottom axis corresponds to 0.1% on the top axis, based on the relation: 100% – 99.9% = 0.1%. Fig. 4 illustrates how the empirical threshold-setting workflow can be extended from manual probability-paper interpretation to MATLAB-based lognormal fitting, which is considered in the following subsections.

Referring to Table 2, which presents a sample of assumed empirical data, the percentage probability of occurrence within the interval (6.0, 6.25) is 0.133%. This value is read directly from the top axis, representing the complemented exceedance probability associated with that threshold range.

The fitted curve to the plotted empirical data will be approximately linear if the percentage probabilities follow a normal distribution. In such cases, the expected false alarm rate may be inferred directly from the plot. For example, an observed rate of approximately 0.07% (or 7×10^{-4}) may be derived, which is seven times higher than a typical design specification of 10^{-4}. However, lower-probability thresholds can be estimated by extrapolating the fitted line to intersect the desired probability level on the y-axis. The corresponding PLD value at this intersection point is then taken as the estimated threshold.

If the underlying system behaviour follows a non-linear or non-Gaussian distribution, the plotted curve may still be smooth but deviate from linearity. Even in such cases, extrapolation can be used to estimate threshold values corresponding to rare-event probabilities, though with greater caution regarding the validity of the fitted model.

Threshold extractionrules

Thresholds are extracted as one-sided predictive intercepts at $\alpha = 10^{-4}$ per operating point from the upper tail of the healthy PLD distribution for each monitored signal, namely motor current, potentiometer output, and tachometer response. The extracted threshold therefore represents the disparity level that is expected to be exceeded only with the specified nuisance-disconnect probability under healthy operation. In this way, threshold selection is linked directly to the acceptable false-alarm risk rather than being chosen arbitrarily.

Model selection follows the behaviour of the probability-plot representation and the quality of the tail fit. A linear probability-paper fit is used when the empirical points remain sufficiently straight in the region of interest, indicating that a normal approximation is adequate for threshold extrapolation. A two-parameter lognormal model is used when the data are non-negative and positively skewed but do not

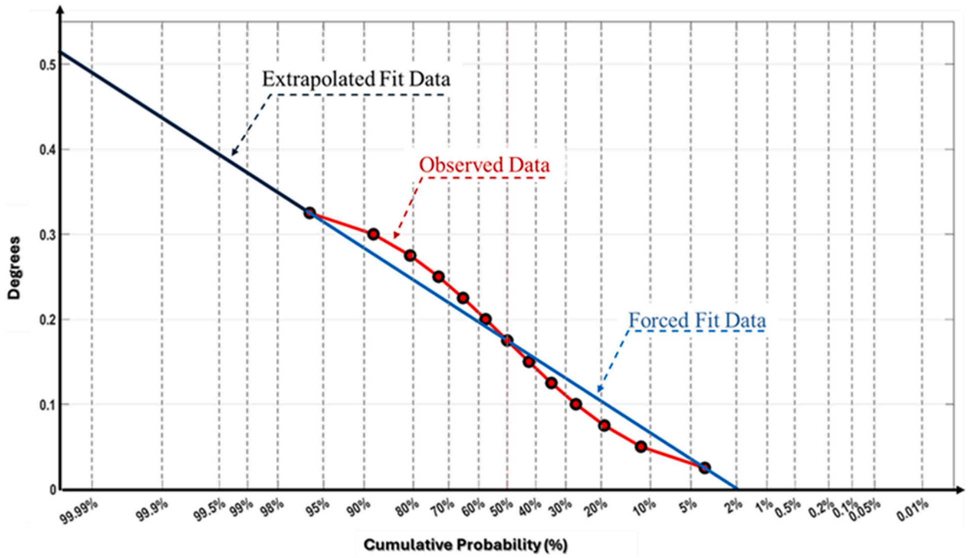

Fig. 4. Lognormal Probability Plot using MATLAB (Observed Data + Forced Fit).

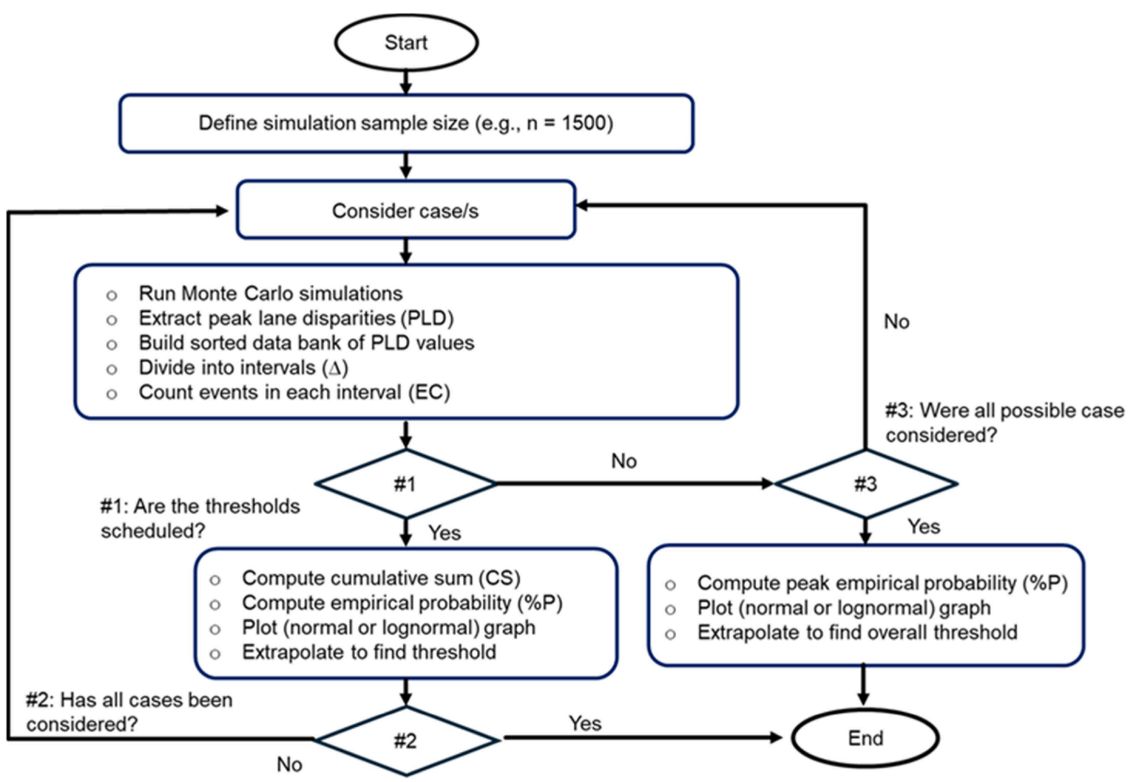

Fig. 5. Flowchart diagram illustrating the Monte Carlo threshold estimation process.

indicate the need for an explicit location shift. A three-parameter lognormal model is used when the empirical tail behaviour suggests that an additional location parameter improves alignment between the fitted curve and the observed data.

Where more than one representation appears plausible, the selected threshold is taken to be the more conservative upper-tail intercept. This rule is adopted because the purpose of the threshold is to protect against under-estimation of rare-event disparities while maintaining a controlled nuisance-disconnect probability. The extracted thresholds are then used either as scheduled thresholds, by repeating the procedure across the operating envelope, or as an unscheduled threshold, by taking the governing maximum value across all operating points.

Thus, the threshold extraction stage formalises what has traditionally been done manually on probability paper by replacing subjective line placement and extrapolation with an explicit, reproducible rule set based on empirical PLD distributions and stated tail-model assumptions. This makes the process more transparent, auditable, and suitable for aerospace EMA monitoring applications.

Normal vs lognormalprobabilityplotsfor thresholdestimation

Normal probability plots provide a simple and interpretable baseline

Table 2
Typical data Setting up the Simulation Graphical Monte Carlo.

Interval (Δ)	Events count (EC)	Cumulative Sum (*CS*)	Probability percentage of occurrence (%*P*)
6.0	2	2	0.133
6.25	2	4	0.27
6.5	7	11	0.73
6.75	48	59	3.93
7.0	132	191	12.73
7.25	178	369	24.6
7.5	256	625	41.67
7.75	232	857	57.13
8.0	197	1054	70.27
8.25	164	1218	81.2
8.5	137	1355	90.33
8.75	76	1431	95.4
9.0	35	1466	97.73
9.25	18	1484	98.93
9.5	9	1493	99.53
9.75	4	1497	99.8
10.0	2	1499	99.93
10.25	1	1500	100

for threshold estimation, particularly when the empirical PLD data remain approximately linear on probability paper. In such cases, the normal approximation offers a straightforward means of extrapolating rare-event thresholds from the upper tail of the healthy distribution. However, in practical EMA applications, PLD data may deviate from linearity because of positive skewness, operating-point dependence, and the combined influence of tolerances, loading, and sensor variation. Under such conditions, a normal probability-paper fit may underestimate the upper tail and lead to thresholds that are insufficiently conservative for low-probability fault-monitoring requirements.

Lognormal probability plots provide a natural extension when the empirical data are strictly non-negative and exhibit skewed behaviour. In the present work, both two-parameter and three-parameter lognormal forms are considered. The two-parameter form is suitable when the data are positive and skewed without requiring a location shift, while the three-parameter form provides added flexibility when the tail behaviour indicates that a shift parameter improves the fit. Comparing the normal, two-parameter lognormal, and three-parameter lognormal representations therefore allows the sensitivity of the extracted threshold to model choice to be examined explicitly.

The purpose of this comparison is not simply to replace normal probability paper with an alternative fit, but to determine when the classical straight-line approximation is adequate and when a lognormal tail model provides a more realistic representation of the healthy PLD distribution. In this way, threshold setting remains grounded in the same graphical engineering logic while becoming more robust to non-Gaussian tail behaviour. The comparison also clarifies how model choice influences conservatism at very low exceedance probabilities, which is critical when thresholds are specified at the $\alpha = 10^{-4}$.

Fig. 6 is the manual probability-paper plot of the empirical PLD data, and Table 3 provides the interval-versus-probability data that underpin that plot. In the manuscript, Table 3 is explicitly titled "Interval vs Probability % Empirical PLD data", so it functions as the numerical basis for the probability-paper representation.

Lognormal modelling,MATLAB-Based overlays,and results

When the empirical peak lane disparity data depart from linearity on normal probability paper, lognormal modelling provides a more flexible representation of the upper tail. This is particularly relevant when the monitored quantities are non-negative and exhibit skewed behaviour, as may occur in the healthy distributions of motor current, potentiometer output, and tachometer response across the operating envelope. In such cases, lognormal probability plots provide a systematic extension of the graphical threshold-setting approach and allow the effect of tail-model choice on extracted thresholds to be examined more explicitly.

A random variable X is said to follow a lognormal distribution if its natural logarithm $Y = \ln(X)$ is normally distributed with mean $\mu$and standard deviation σ. The corresponding PDF is given by

Table 3
Interval vs Probability % Empirical PLD data.

Potentiometer Data		Tachometer Data		Current Data	
Interval (degree)	Prob%	Interval (degree /sec)	Prob %	Interval (Amps)	Prob %
0	0.47	−0.0625	0.07	0	0.07
0.025	6.13	0.0625	2.93	0.5	5.93
0.05	18.53	0.1875	11.73	1	22.20
0.075	36.00	0.3125	26.07	1.5	44.87
0.1	54.67	0.4375	41.87	2	63.20
0.125	71.20	0.5625	61.73	2.5	78.80
0.15	82.87	0.6875	76.20	3	87.73
0.175	92.53	0.8125	87.33	3.5	93.67
0.2	96.13	0.9375	94.93	4	96.93
0.225	98.13	1.0625	97.47	4.5	98.87
0.25	99.33	1.1875	99.00	5	99.27
0.275	99.87	1.3125	99.60	5.5	99.60
0.3	100.00	1.4375	99.80	6	99.87
0.325	100.00	1.5625	99.87	6.5	99.93

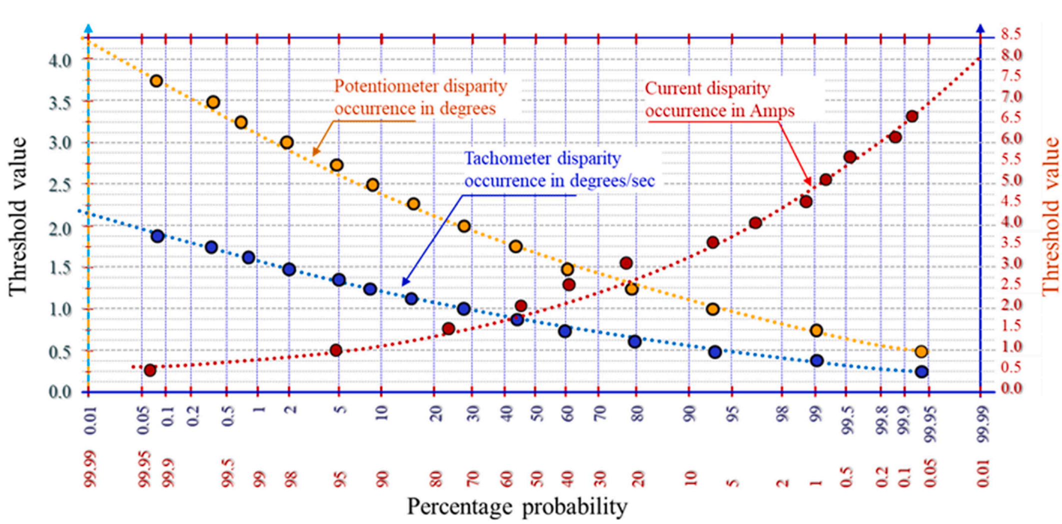

Fig. 6. Manual Probability Plot of Peak Disparities.

$$f(x;\mu,\sigma) = \frac{1}{x\sigma\sqrt{2\pi}} exp\left(-\frac{(\ln x-\mu)^2}{2\sigma^2}\right), x>0 \quad (2)$$

and the cumulative distribution function (CDF) is:

$F(x;\mu,\sigma) = \Phi\left(\frac{(\ln x-\mu)}{\sigma}\right)$, where $\Phi(.)$ denotes the standard normal CDF.

In the present study, both two-parameter and three-parameter lognormal forms are considered. The two-parameter model is appropriate when the data are positive and skewed without requiring a location shift, whereas the three-parameter form introduces an additional shift parameter to improve alignment when the empirical tail departs from the simpler model. The purpose of introducing these models is not to replace the underlying engineering logic of probability-paper thresholding, but to provide a more reproducible and auditable basis for threshold extrapolation when the normal approximation is inadequate.

MATLAB is used to support this process through tool-based fitting and visual comparison of empirical data with candidate tail models. In practical implementation, the lognormal model parameters (μ, σ) may be estimated using MATLAB's statistical toolbox [13]. The command `lognfit(data)` returns the maximum-likelihood estimates of μ and σ, while functions such as `lognpdf`, `logncdf`, and `probplot('lognormal',data)` enable direct comparison with normal probability plots and support threshold extraction at specified rare-event probabilities.

The empirical datasets used in this stage are those generated from the simulation procedure and organised in cumulative probability form. Table 3 summarises the interval-versus-probability empirical PLD data used for this purpose.

The plots in Fig. 7 show MATLAB-based overlays in which straight-line, two-parameter lognormal, and three-parameter lognormal fits are superimposed on the empirical data. These overlays allow direct comparison between manual probability-paper interpretation and automated fitting [13–15]. MATLAB-based fitting is therefore used to provide a more reproducible basis for low-probability threshold estimation [13–15].

To demonstrate the approach, the potentiometer dataset from Table 3 is used as an example. Fig. 8 presents the empirical cumulative distribution in engineering units, with potentiometer displacement in degrees on the x-axis together with three fitted models: a linear CDF obtained from a straight-line probability-paper fit, and 2p and 3p lognormal CDFs. Within the observed $0 \sim 0.3^\circ$ range, the empirical points track the lognormal curves closely, indicating that a lognormal representation provides a suitable statistical description of the data. The linear fit remains useful as a transparent engineering approximation, but it is not a true probability model. The 2p lognormal provides a standard skewed distribution without offset, while the 3p lognormal introduces a shift parameter that can improve tail alignment when offset effects are present.

When extrapolated into the extreme $99.9 - 99.99\%$ tail region, the fitted models diverge. For the potentiometer data, the linear and 3p lognormal models remain closer to the empirical behaviour in the observed range, while the 2p lognormal underestimates the mid-range probabilities. In the extreme tail, however, the 2p lognormal predicts the highest thresholds, followed by the 3p lognormal, with the linear fit lowest. Although these differences are numerically modest, they are important in actuator fault detection because underestimation can increase nuisance disconnects or reduce monitoring reliability. Taken together, Fig. 9 shows that the probability-paper straight line provides continuity with classical practice, whereas the lognormal models provide a more flexible and statistically defensible basis for low-probability extrapolation.

The same modelling framework was then applied to the tachometer and current datasets to assess consistency across multiple sensing modalities. Figs. 9∼11 present the MATLAB-based overlays for the potentiometer, tachometer, and current datasets, comparing the empirical data with linear regression and 3p lognormal fits. In each case, the empirical points align well with the fitted trends, supporting the suitability of lognormal modelling and enabling extrapolation to rare-event thresholds. The 3*p* lognormal fit consistently predicts higher upper-tail intercepts than the linear fit, illustrating the sensitivity of threshold values to model choice.

As summarised in Table 4, the potentiometer dataset yields an estimated threshold of approximately 0.30° from the linear fit and approximately 0.35° from the 3p lognormal fit. The tachometer dataset gives approximately $1.62^\circ/s$ from the linear fit and approximately $1.90^\circ/s$ from the 3p lognormal fit, while the current dataset yields

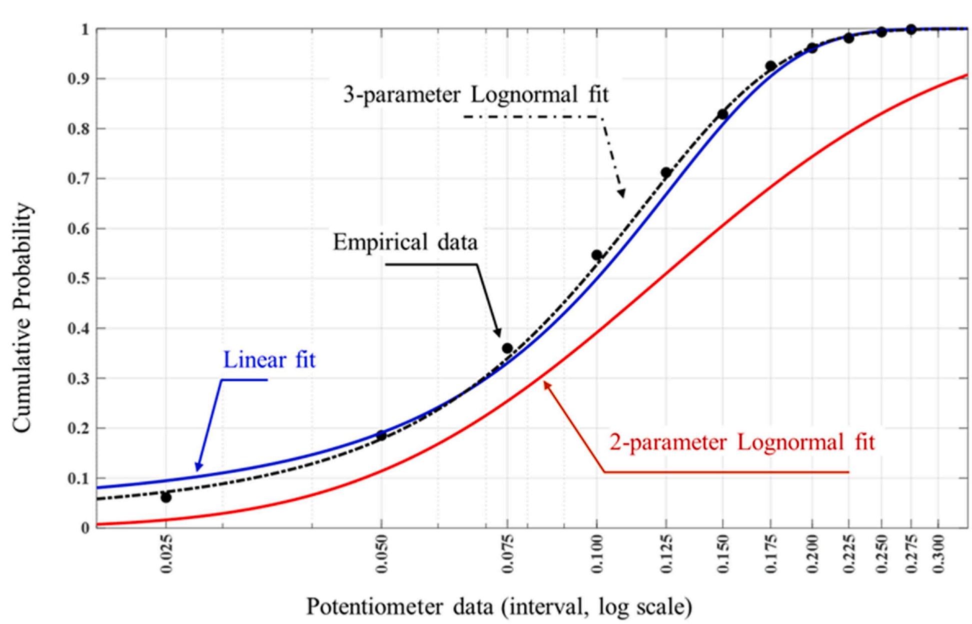

Fig. 7. Lognormal potentiometer empirical cumulative distribution with fit overlays.
The black points show the empirical cumulative probabilities. The overlays are the: Linear CDF, 2-parameter lognormal (2p) CDF, and 3-parameter lognormal (3p) CDF. The y-axis is true probability (0∼1), and x-axis correspond to measured intervals.

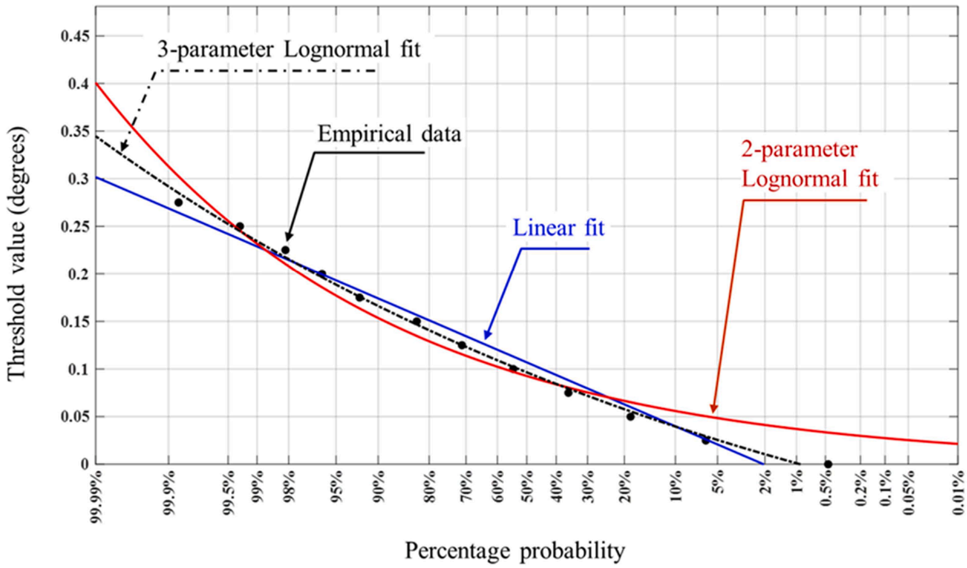

Fig. 8. Lognormal probability plot of potentiometer cumulative data.
Empirical points are compared with extrapolated Linear, 2-parameter and 3-parameter lognormal fit overlays to calculate 10^{-4} inherent potentiometer disparities.

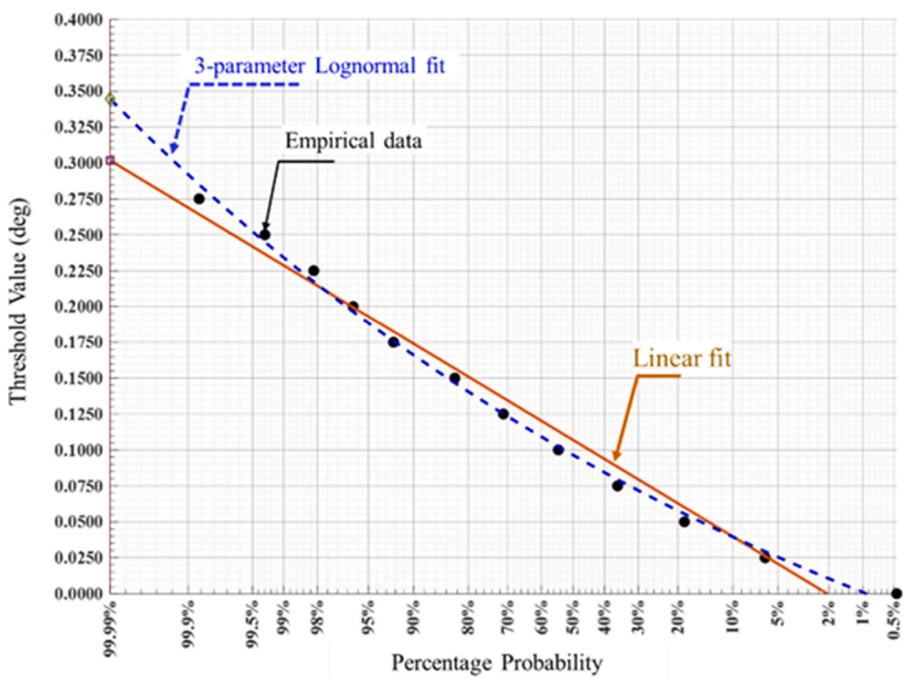

Fig. 9. Potentiometer: Lognormal probability plot comparing empirical points are overlaid with the Linear fit and the 3p lognormal curve.
The high-percentile intercepts illustrate the threshold difference: 3p lognormal $\approx 0.35^{\circ}$ versus linear $\approx 0.30^{\circ}$ The 3p fit provides a more conservative upper-tail estimate.

approximately 6.2 A from the linear fit and approximately 7.9 Amperes from the 3p lognormal fit. These results reproduce the same overall trend observed from manual probability-paper interpretation: the empirical PLD data follow a lognormal tendency, and the 3p lognormal representation generally produces a more conservative upper-tail threshold than the linear approximation.

The MATLAB-based approach offers several advantages over manual plotting. It reduces the subjectivity associated with hand-drawn best-fit lines, enables reproducible extrapolation to very low exceedance probabilities, and allows direct comparison of linear and lognormal models within a consistent numerical framework. The agreement between the manual and MATLAB-based probability plots supports the suitability of the lognormal assumption for the PLD datasets considered here, while the MATLAB-based method extends the analysis with greater accuracy, reproducibility, and traceability. For this reason, it provides the preferred basis for threshold determination in safety-critical actuator applications.

Comparative evaluation

This section compares the strengths and limitations of normal and lognormal probability-based threshold estimation. The emphasis is on the trade-off between the simplicity and transparency of normal probability plotting and the improved tail fidelity of lognormal models when

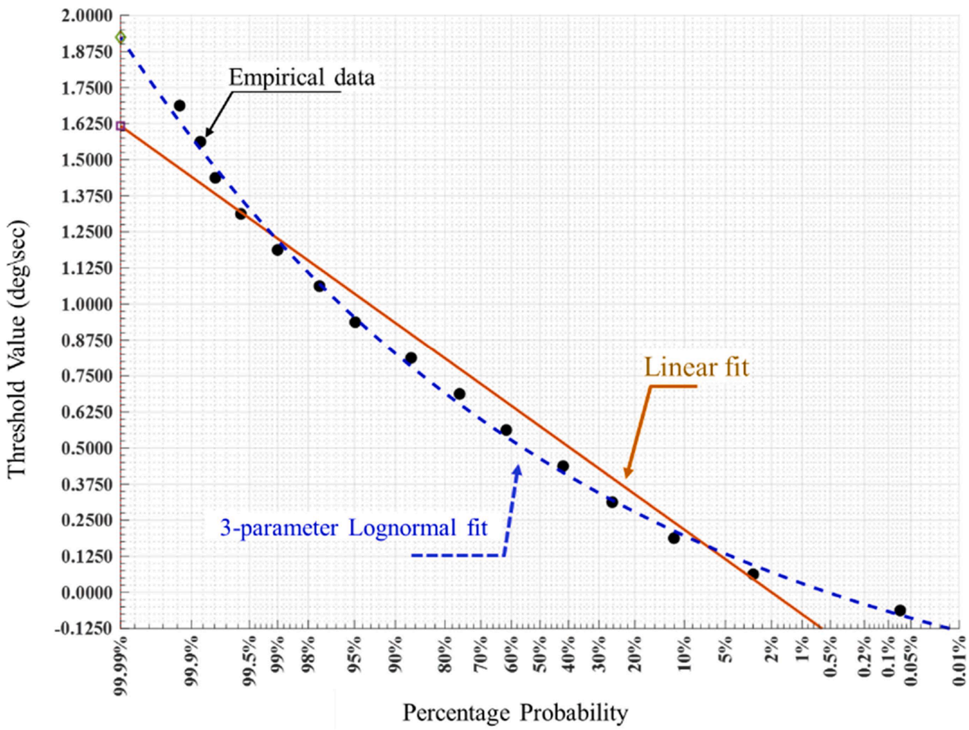

Fig. 10. Tachometer: Lognormal probability plot comparing empirical data, Linear fit, and 3p lognormal curve.
Left-border intercepts: 3p ≈ 1.9 versus Linear ≈ 1.62.The 3p fit yields a higher tail threshold and better alignment in the upper percentiles.

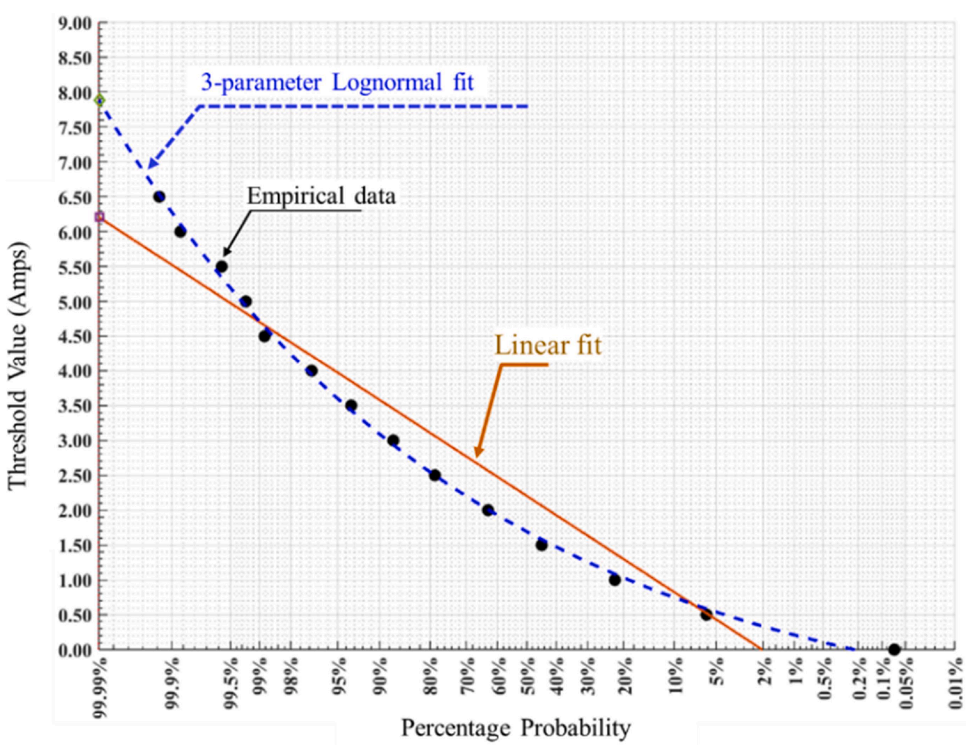

Fig. 11. Current: Lognormal probability plot comparing empirical data, Linear fit, and 3p lognormal curve.
Left-border intercepts: 3p ≈ 7.9 versus Linear ≈ 6.2 (amperes). The 3p model provides the more conservative tail estimate.

the empirical PLD distributions are positively skewed.

Normal probability plotting is simple, widely understood, and effective when the underlying distribution is approximately symmetric [9]. Its main advantage is transparency, since thresholds can be interpreted directly from the fitted straight line. However, when the empirical data are skewed, it can underestimate upper-tail thresholds. In contrast, lognormal modelling, particularly when implemented in MATLAB [16,17], provides a more flexible representation of positively skewed PLD data and improves threshold estimation at low exceedance probabilities. This gain in fidelity comes at the cost of added modelling

Table 4
Observed thresholds from MATLAB-based overlays comparing empirical data with both the Linear regression and the 3p lognormal fits.

Dataset	Linear fit	3p Lognormal fit
Potentiometer (Fig. 9)	$\sim 0.3^o$	$\sim 0.35^o$
Tachometer (Fig. 10)	$\sim 1.62^o/sec$	$\sim 1.9^o/sec$
Current (Fig. 11)	~6.2 Amps	~7.9 Amps

and fitting complexity.

The choice of method should therefore be guided by the statistical behaviour of the data and the criticality of accurate tail estimation in the intended application. For high-integrity aerospace EMA monitoring, the results of the present study indicate that lognormal-based fitting provides a more conservative and reproducible basis for threshold determination, while normal probability paper remains useful as a transparent baseline and interpretive tool.

Outlook: AI-based thresholdingand controlconsiderations

AI-based and predictive thresholding

The threshold-setting framework developed in this paper is based on explicit statistical modelling of the PLD distributions and therefore provides a suitable foundation for adaptive extensions. An important direction for future work is the integration of lognormal-based threshold modelling with AI-assisted predictive thresholding. The objective is to explore how machine-learning methods may adapt thresholds in real time under changing operating conditions, while maintaining fault sensitivity and limiting false alarms.

Lognormal modelling is valuable in this context because it captures skewness and tail behaviour that are important for rare-event threshold estimation [16]. MATLAB-based fitting also provides statistical diagnostics, including confidence intervals and goodness-of-fit measures, which could support future predictive implementations [17]. This framework may be extended through machine-learning techniques [18, 19], in which model parameters or threshold levels are updated using real-time operational data. Such an approach could improve resilience to drift, preserve sensitivity to emerging faults, and support a transition from conventional threshold-based fault detection toward predictive threshold management in aerospace EMAs.

Control architecture considerations. Although control-system design is not the main focus of this paper, it is briefly mentioned because the monitored signals used for threshold setting arise within that control framework. The thresholds derived in this study are governed primarily by inherent lane disparities rather than by the nominal system response itself.

Conclusion

This paper presented a simulation-based graphical Monte Carlo workflow for setting sensor thresholds in multi-lane electromechanical actuator systems. By combining Monte Carlo-generated peak lane disparity data with probability-plot-based threshold extraction, the method provides a structured and auditable alternative to manual probability-paper extrapolation. The approach enables threshold values to be derived at specified nuisance-disconnect probabilities while preserving transparency in the relationship between empirical data, tail modelling, and the resulting threshold estimates.

The methodology was demonstrated on a representative aerospace case study based on a multi-lane EMA associated with the Sea Harrier inboard aileron. The results showed that threshold estimates are sensitive to tail-model choice, particularly at low exceedance probabilities relevant to high-integrity monitoring. Normal probability-paper fits provide a transparent baseline, whereas lognormal modelling, supported by MATLAB-based fitting and overlays, offers a more flexible and generally more conservative basis for threshold estimation when the empirical PLD distributions are positively skewed.

Overall, the study shows that threshold setting can be treated as a reproducible engineering workflow rather than a subjective manual exercise. Future work will focus on hardware-in-the-loop validation, real-time implementation, and adaptive threshold management using data-driven and AI-assisted approaches for safety-critical EMA applications.

Data availability

The data supporting the findings of this study are available from the corresponding author upon reasonable request.

CRediT authorship contribution statement

Fawaz Yahya Annaz: Conceptualization, Data curation, Formal analysis, Funding acquisition, Investigation, Methodology, Project administration, Resources, Software, Supervision, Validation, Visualization, Writing – original draft, Writing – review & editing.

Declaration of competing interest

The authors declare that they have no known competing financial interests or personal relationships that could have appeared to influence the work reported in this paper.

The authors declare the following financial interests/personal relationships which may be considered as potential competing interests:

Dr Fawaz Annaz reports a relationship with Birmingham City University that includes: employment. If there are other authors, they declare that they have no known competing financial interests or personal relationships that could have appeared to influence the work reported in this paper.

References

[1] G. Qiao, G. Liu, Z. Shi, Y. Wang, S. Ma, T.C. Lim, A review of electromechanical actuators for more all Electric aircraft systems, Proc. Inst. Mech. Eng. C: J. Mech. Eng. Sci. 232 (22) (2018) 4128–4151.
[2] F.Y. Annaz, M.M. Kaluarachchi, Progress in redundant electromechanical actuators for aerospace applications, Aerospace 10 (787) (2023).
[3] Z. Yin, N. Hu, J. Chen, Y. Yang, G. Shen, A review of fault diagnosis, prognosis and health management for aircraft electromechanical actuators, IET Electr. Power Appl.; IET Electr. Power Appl. 16 (11) (2022) 1249–1272.
[4] D. Arriola, F. Thielecke, Model-based design and experimental verification of a monitoring concept for an active-active electromechanical aileron actuation system, Mech. Syst. Signal. Process. 94 (2017) 322–345.
[5] D. Vedova, M. Germanà, A. Berri, P.C. Ma, Model-based fault detection and identification for prognostics of electromechanical actuators using genetic algorithms, Aerospace 6 (94) (2019).
[6] R. Rubinstein, Simulation and the Monte Carlo Method, John Wiley & Sons Inc., 1981.
[7] R.Y. Rubinstein, D.P. Kroese, Simulation and the Monte Carlo Method, 2, John Wiley & Sons, 2017.
[8] J. Fu, J.-C. Mare, L. Yu, Y. Fu, Multi-level virtual prototyping of electromechanical actuation system for more electric aircraft, Chin. J. Aeronaut. 31 (5) (2018) 892–913.
[9] J.M. Chambers, W.S. Cleveland, B. Kleiner, P.A. Tukey, Graphical Methods for Data Analysis, Wadsworth International Group, Belmont, California, 1983.
[10] J. Smith, R. Brown, Fault detection and isolation in aerospace actuation systems, J. Aerosp. Eng. 25 (3) (2012) 123–135.
[11] Y. Lin, E.A. Baumann, D.M. Bose, R. Beck, G.D. Jenney, Tests and Techniques for Characterizing and Modeling X-43A Electromechanical Actuators, NASA Technical Memorandum NASA/TM-2008-214637, 2008.
[12] RTCA, DO-160G, Environmental Conditions and Test Procedures For Airborne Equipment, RTCA, Inc., Washington, D.C., 2010.
[13] N.L. Johnson, S. Kotz, N. Balakrishnan, Continuous Univariate Distributions, 1, Wiley, 1994.
[14] J.F. Lawless, Statistical Models and Methods for Lifetime Data, Wiley, 2003.
[15] NIST/SEMATECH, NIST/SEMATECH E-Handbook of Statistical Methods (Section 6.3.6, Probability Plots), 2023.
[16] J. Aitchison, J.C. Brown, The Lognormal Distribution, Cambridge University Press, Cambridge, 1957.

[17] MathWorks Inc., “MATLAB Statistics and Machine Learning Toolbox User’s Guide,” Natick, MA, 2024.
[18] Y. Lei, B. Yang, X. Jiang, F. Jia, N. Li, A.K. Nandi, Applications of machine learning to machine fault diagnosis: a review and roadmap, Mech. Syst. Signal. Process. 138 (2020) 106587. VolsArticle.
[19] W. Zhang, D. Yang, H. Wang, Data-driven methods for predictive maintenance of industrial equipment: a survey, IEEE Syst. J. 13 (3) (2019) 2213–2227.